

Preparation of an Exciton Condensate of Photons on a 53-Qubit Quantum Computer

LeeAnn M. Sager, Scott E. Smart, and David A. Mazziotti*

Department of Chemistry and The James Franck Institute, The University of Chicago, Chicago, IL 60637

(Dated: Submitted April 28, 2020)

Quantum computation promises an exponential speedup of certain classes of classical calculations through the preparation and manipulation of entangled quantum states. So far most molecular simulations on quantum computers, however, have been limited to small numbers of particles. Here we prepare a highly entangled state on a 53-qubit IBM quantum computer, representing 53 particles, which reveals the formation of an exciton condensate of photon particles and holes. While elusive for more than 50 years, such condensates were recently achieved for electron-hole pairs in graphene bilayers and metal chalcogenides. Our result with a photon condensate has the potential to further the exploration of this new form of condensate that may play a significant role in realizing efficient room-temperature energy transport.

Exciton condensation is defined by the condensation of particle-hole pairs (excitons) into a single quantum state to create a superfluid. The superfluidity of electron-hole pairs—while, by definition, incapable of involving either the frictionless flow of matter or charge—does involve the non-dissipative transfer of energy [1, 2]. As such, understanding and exploiting the superfluid properties of exciton condensates may be instrumental in the effort to design wires and electronic devices with minimal loss of energy. Consequently, considerable theoretical and experimental investigation has centered on exciton condensation in recent years [1, 3–8].

While excitons form spontaneously in semiconductors and insulators and while the binding energy of the excitons can greatly exceed their thermal energy at room temperature, they recombine too quickly to allow for formation of a condensate in a simple manner. To combat recombination, the coupling of excitons to polaritons—which requires the continuous input of light [9, 10]—and the physical separation of electrons and holes into bilayers—which involves impractically high magnetic fields and/or low temperatures [3, 4, 10–12]—are employed. Thus, a new, more-practical avenue for the creation of exciton condensates and the study of their properties is desired.

Computation has recently been employed to explore strongly-correlated quantum matter [13], as superconducting circuits allow for precise manipulation of the strongly-interacting qubits to create specified quantum states populated by microwave photons. Here we prepare and measure an exciton condensate of photons on a quantum computer. Quantum computation should be particularly adapted to the exploration of exciton condensation as the binary nature of an individual qubit can be interpreted as a site consisting of one fermion and two orbitals; extrapolating, a system of N qubits can be viewed as N degenerate sites each consisting of one fermion and two orbitals. We use such a Hamiltonian of N -fermions in two N -degenerate levels, known as

the Lipkin Hamiltonian [14–18], to prepare a molecular-scale exciton condensate by tuning its interaction parameter to the large-coupling limit. Because each transmon qubit on the quantum computer utilized for this study employs a microwave photon in an anharmonic quantum well potential, the exciton condensates we construct are comprised of photon-hole pairs condensing into single quantum states—i.e., exciton condensates of photons on a quantum computer.

We use the theoretical signature of exciton condensation—derived by Rosina and Garrod [5, 19]—to probe the extent of exciton condensation for a wide range of preparations through simulation and physical quantum computation experiments. From analysis of the natural occupation numbers of these preparations, we establish that prepared states with orbital occupation numbers consistent with the Greenberger-Horne-Zeilinger (GHZ) state—including but not limited to the GHZ state—demonstrate maximal exciton condensation for three qubits. Further, we establish through simulation that for any number of qubits, the GHZ state exhibits maximal character of exciton condensation, demonstrating that the “maximal entanglement” of the GHZ state—for all N —corresponds to the entanglement of particle-hole pairs. Through preparing and probing the GHZ states on quantum devices, character of exciton condensation is experimentally observed in systems composed of up to fifty-three qubits, although decoherence in the higher-qubit systems leads to multiple eigenstates demonstrating excitonic character instead of a single, maximally-entangled eigenstate. Specifically as the GHZ state is prepared here on transmon qubits and is hence occupied by microwave photons, exciton condensation of photons—i.e., the entanglement of photon-hole pairs—is experimentally observed for systems of three to fifty-three qubits.

Results:

Establishing signature of exciton condensation.

Condensation phenomena has been an active area of research since 1924 when Einstein and Bose first introduced their ideal “Bose-Einstein” gas [20, 21]. The identical particles comprising this gas—bosons—are able to aggregate into a single quantum ground state when suffi-

* damazz@uchicago.edu

ciently cooled [21], which leads to superfluidity of the constituent bosons [22, 23]. In 1940, Pauli established the relationship between spin and statistics, demonstrating that particles with integral spin values (bosons) obey Bose-Einstein statistics and hence may form a condensate [24]. Particles with half-integer spins (fermions), in contrast, must obey the Pauli exclusion principle and are therefore unable to condense into a single quantum state to form a condensate. However, pairs of fermions—forming an overall bosonic state—can condense. In a system of fermionic particles, this pairing can be accomplished through either particle-particle or particle-hole pairing. The condensation of particle-particle pairs into a single quantum state is termed fermion-pair condensation with the resultant superfluidity of fermion pairs causing superconductivity [25]; likewise, the condensation of particle-hole pairs (excitons) into a single quantum state is termed exciton condensation with the resultant superfluidity of exciton pairs causing the nondissipative transfer of energy [1].

In order to computationally probe the presence and extent of condensation behavior, it is useful to establish a calculable, characteristic property. As proven independently by Yang and Sasaki [26, 27], the quantum signature of fermion condensation is associated with a large eigenvalue of the particle-particle RDM with elements given by

$${}^2D_{k,l}^{i,j} = \langle \Psi | \hat{a}_i^\dagger \hat{a}_j^\dagger \hat{a}_l \hat{a}_k | \Psi \rangle \quad (1)$$

where $|\Psi\rangle$ is an N -fermion wavefunction, the roman indices correspond to one-fermion orbitals in a finite basis set with rank r , and \hat{a}^\dagger and \hat{a} are fermionic creation and annihilation operators respectively. We denote the largest eigenvalue of the particle-particle RDM as λ_D and use this value as a signature of the extent of fermion pair condensation, with values above one demonstrating condensation.

In analogy to the signature of fermion pair (particle-particle) condensation being a large eigenvalue of the particle-particle RDM, one may assume the quantum signature of exciton (particle-hole) condensation to be a large eigenvalue in the particle-hole RDM [5, 19, 28] with elements given by

$${}^2G_{k,l}^{i,j} = \langle \Psi | \hat{a}_i^\dagger \hat{a}_j \hat{a}_l^\dagger \hat{a}_k | \Psi \rangle. \quad (2)$$

However, there exist two large eigenvalues for the particle-hole RDM, one of which corresponds to a ground-state-to-ground-state transition (not exciton condensation). In order to eliminate this extraneous large eigenvalue, the modified particle-hole matrix with the ground-state resolution removed

$${}^2\tilde{G}_{k,l}^{i,j} = {}^2G_{k,l}^{i,j} - {}^1D_k^i {}^1D_l^j \quad (3)$$

is constructed. Garrod and Rosina [19] have shown that—for an N -fermion system—the eigenvalues of the ${}^2\tilde{G}$ matrix are zero or one in the non-interacting limit

and bounded above by $\frac{N}{2}$ in the limit of strong correlation. We denote the largest eigenvalue of the modified particle-hole RDM as λ_G and use this value as a signature of the presence and extent of exciton condensation.

Exploration of λ_G for Three-Qubit Preparations. Three-qubit systems—which correspond to three fermions in six orbitals—are the smallest systems to possess nontrivial classes of entanglement. Hence, in this study, these minimally-small, three-qubit systems are first thoroughly explored in order to obtain insights on the preparation and characteristics of exciton condensates that are later employed to guide the investigation of larger-qubit systems.

To this end, the three-qubit preparation

$$|\Psi\rangle = C_3^2 R_{y,3}(\theta_3) C_1^2 R_{y,1}(\theta_2) C_1^3 R_{y,1}(\theta_1) |000\rangle, \quad (4)$$

which—as shown in Ref. 29—is a minimalistic three-qubit preparation known to effectively span all real, 1-qubit occupations, is utilized to systematically prepare all real, three-qubit quantum states up to local unitaries. Note that in this preparation, $|000\rangle$ represents the initial all-zero qubit state, C_i^j is a controlled-NOT (CNOT) gate with i control and j target, and $R_{y,i}(\theta)$ is a $\frac{\theta}{2}$ angle rotation about the y -axis of the Bloch sphere on the i^{th} qubit. By scanning over the angles of rotation ($\theta_1, \theta_2, \theta_3$), we prepare states with all possible, real qubit occupation numbers and hence sweep through all possible correlation phenomena. By probing λ_G for each of the prepared states, we then determine the extent of exciton condensation for all three-qubit correlation.

Orbital occupation numbers—obtained from the eigenvalues of the one-fermion RDM—are used as a practical coordinate representation in which to visualize λ_G for all electron correlations (all possible occupations). For a three-qubit system, a pure quantum system of three electrons in six orbitals, these occupations are constrained beyond the traditional Pauli constraints ($0 \leq n_i \leq 1$) [30]. For a three-qubit quantum system, these relevant so-called generalized Pauli constraints are

$$n_5 + n_6 - n_4 \geq 0 \quad (5)$$

where

$$n_1 + n_6 = 1 \quad (6)$$

$$n_2 + n_5 = 1 \quad (7)$$

$$n_3 + n_4 = 1 \quad (8)$$

in which each n_i corresponds the natural-orbital occupations ordered from largest to smallest [31–34]. The three, independent eigenvalues, n_4, n_5 , and n_6 , can be used as a three-coordinate representation of a given quantum state against the Pauli polytope, the set of all possible occupations according to the Pauli constraints ($0 \leq n_i \leq 1$), as well as the generalized Pauli polytope, the set of all possible occupations according to the generalized Pauli constraint (Eq. (5)). [See Fig. 1.]

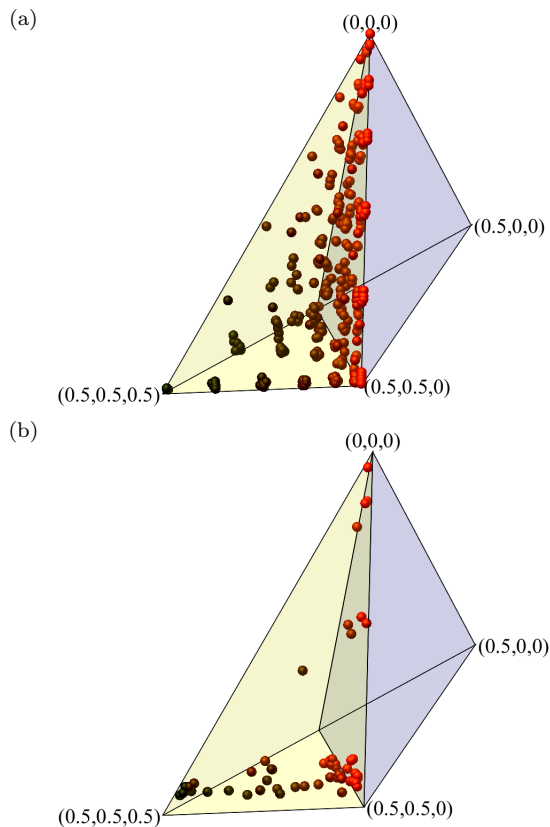


FIG. 1: **Exciton Condensation in the Generalized Pauli Polytope.** (a) Simulated and (b) experimental data shows that the occupation numbers (n_4 , n_5 , n_6) of the 1-RDM lie in the generalized Pauli polytope (yellow region) with exciton condensate character (darkening red indicates an increasing λ_G) emerging as the occupations saturate the vertex $(0.5, 0.5, 0.5)$.

Scatter plots of the occupation numbers for simulated and mitigated, experimental calculations (see Methodology for discussion on error mitigation) are shown in Fig. 1 against the Pauli polytope (the combination of the yellow and blue regions allowed by $0 \leq n_i \leq 1$) and the generalized Pauli polytope (only the yellow region allowed by Eq. (5)). For the simulated calculations (Fig. 2a), possible combinations of angles θ_1 , θ_2 , and θ_3 , varied systematically for $\theta \in [0, \frac{\pi}{2}]$, are used to prepare quantum states according to Eq. (4). Note that the darker the color red for a sphere in the figure, the larger the λ_G value associated with the given calculation. As can be seen from Fig. 1, while the preparations span all orbital occupations consistent with the generalized Pauli constraints and hence all electron correlations, only values approaching the $(n_4, n_5, n_6) = (0.5, 0.5, 0.5)$ corner of the polytope, known to be the occupations of the GHZ state, demonstrate maximal exciton condensation. The mitigated, experimental results shown in Fig. 2b in which θ_1 is constrained to either 0 or $\frac{\pi}{2}$ to limit computational expense confirm the simulation results.

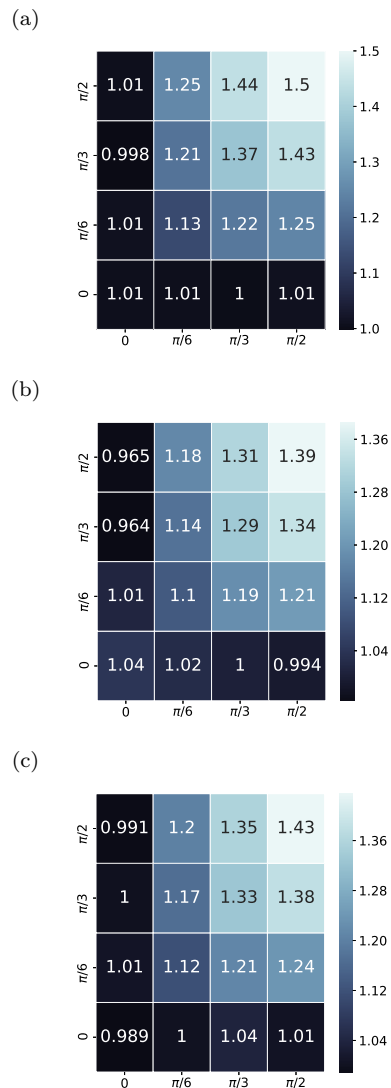


FIG. 2: **Large Particle-hole Eigenvalues and Exciton Condensation.** The largest eigenvalue λ_G of the modified particle-hole density matrix is shown as a function of the preparation angles θ_2 and θ_3 in the range $[0, \frac{\pi}{2}]$ with $\theta_1 = 0$ in Eq. (4) for (a) simulated calculations, (b) experimental results, and (c) mitigated, experimental results.

In order to better visualize the variation of exciton condensate character with respect to variation in the preparation of the qubit quantum state, one particular scan of λ_G for the minimalistic three-qubit state preparation is shown in Fig. 2 in which the θ_1 value is set to zero and the other angles are varied systematically from 0 to $\frac{\pi}{2}$ with a $\frac{\pi}{6}$ interval. In Fig. 2, results are given for (a) simulation, (b) experiments without mitigation, and (c) mitigated experiments. Note that these particular scanning parameters are chosen as they well-represent the observed range in λ_G and demonstrate the maximal three-qubit λ_G of $\frac{N}{2} = \frac{3}{2} = 1.5$ for the simulated re-

N	$\lambda_G^{sim.}$	$\lambda_G^{mit.}$	$\lambda_G^{exp.}$
3	1.50	1.44	1.39
4	2.00	1.92	1.80
5	2.50	2.33	2.22
6	3.00	2.70	2.27
7	3.50	—	2.44
8	4.00	—	2.72
9	4.50	—	2.73
10	5.00	—	2.93
11	5.50	—	3.08
12	6.00	—	3.22
13	6.50	—	3.28
14	7.00	—	3.25
15	7.50	—	2.91 ^a
16	8.00	—	2.28
22	11.0	—	2.68
28	14.0	—	3.48
34	17.0	—	3.25
39	19.5	—	2.71
47	23.5	—	2.77
53	26.5	—	3.07 ^a

TABLE I: Eigenvalue table for the ${}^2\tilde{G}$ matrix for simulated ($\lambda_G^{sim.}$), mitigated experimental ($\lambda_G^{mit.}$), and experimental ($\lambda_G^{exp.}$) GHZ state results

^a No suitable circuit orientation on quantum device for creation of a 15 qubit GHZ state, introducing excess error to the calculation.

sults. Additionally, note that even the unmitigated, experimental results [(b)] demonstrate a relatively large λ_G of 1.39, a clear demonstration of exciton condensate character despite experimental errors (see Methods for discussion of errors). This large, non-error-corrected signature of exciton condensation shows that exciton condensation is indeed created on the quantum computer and is not an artifact of error correction. The large eigenvalue λ_G and the degree of saturation of the generalized Pauli constraint in Eq. (5) are reported in Tables IV through VIII and Fig. 1 for many sets of orbital occupations in the Supporting Information.

Exploration of λ_G for GHZ State. As shown above, the region of the Pauli polytope associated with the GHZ state, the state described by

$$|\Psi_{GHZ}\rangle = \frac{1}{\sqrt{2}} (|0\rangle^{\otimes N} + |1\rangle^{\otimes N}) \quad (9)$$

for an N -qubit system, demonstrates maximal exciton condensate character for three qubits; however, the minimalistic preparation used to probe λ_G permits only double excitations, precluding the measurement of λ_G associated with the true GHZ state for three qubits. Therefore, a different qubit preparation scheme is used to generate the three-qubit GHZ state (see the Methods section). The maximum exciton condensate character ($\frac{N}{2} = \frac{3}{2} = 1.5$) is indeed observed for simulation of the three-qubit GHZ state.

The GHZ qubit preparation is generalizable to any N -qubit state, allowing for the extension of the above result to larger numbers of qubits, the outcomes of which can

be seen in Table I. These results demonstrate that the beginnings of exciton condensation is achieved on quantum computers using 3-to-53 qubits. Note that error mitigation is only feasible for systems with $N \leq 6$ qubits as larger-qubit error mitigation schemes necessitate more circuits than the experimental quantum devices allow. Additionally, to limit computational expense, only real contributions to the reduced density matrices are computed. See the Methods section for specific experimental details and Tables II, III, and IV in the Supporting Information for device specifications.

As is apparent from simulated results (Table I and Fig. 3a), the GHZ state for all qubits approaches the maximal value for exciton condensate character of $\frac{N}{2}$. As such, the GHZ state is expected to demonstrate maximal exciton condensation for a given number of qubits. While the experimental results in Table I and Fig. 3b do not achieve maximal λ_G values, although the error-mitigated results do appear to approach $\frac{N}{2}$, exciton condensation character ($\lambda_G > 1$) is observed for each GHZ state prepared for $N = 3$ -to-53 qubits.

The larger deviation from the simulated results observed in the higher-qubit experiments—in which there seems to be a maximal signature of exciton condensation of around $\lambda_G \approx 3$ (Table I and Fig. 3b)—is likely due to the cumulative effects of errors that become increasingly significant as the number of qubits—and hence the number of CNOT gates applied—increases. (See the Supporting Information for details of gate errors, readout errors, and multi-qubit CNOT errors for the quantum devices employed for experimentation.) These errors seem to prevent the formation of a global excitonic state due to dispersion; however, as the number of qubits is increased, the condensation behavior of the N -qubit system does still increase as is shown in Fig. 3c. In these higher-qubit experiments, there are multiple eigenvalues of the ${}^2\tilde{G}$ matrix above one, indicating that there are multiple eigenstates demonstrating character of exciton condensation. The sum of the eigenvalues above one increases in an almost linear fashion as the number of qubits is increased, demonstrating an overall increase in the excitonic nature of the prepared states even if maximal condensation behavior in a single orbital can not be obtained for these higher-qubit experiments due to dispersion.

The GHZ state is often referred to as a “the maximally-entangled state” as it has maximum entanglement entropy [35]; however, there are diverse types of non-equivalent multi-partite entanglement. For example, Bose-Einstein condensation, fermion pair condensation, and exciton condensation are all phenomena that occur due to the entanglement of bosons, differing in their signatures and the types of bosons that are entangled. Here we have demonstrated a new characteristic of the maximal entanglement of the GHZ state—namely the maximal entanglement of particle-hole pairs (excitons). Further, the fermion pair condensate character (λ_D) is additionally probed for the GHZ state, and no fermion pair condensation is observed ($\lambda_D < 1$). (See Fig. 3.) As

such, we have shown that the maximal entanglement of the GHZ state does not correspond to the entanglement of particle-particle pairing.

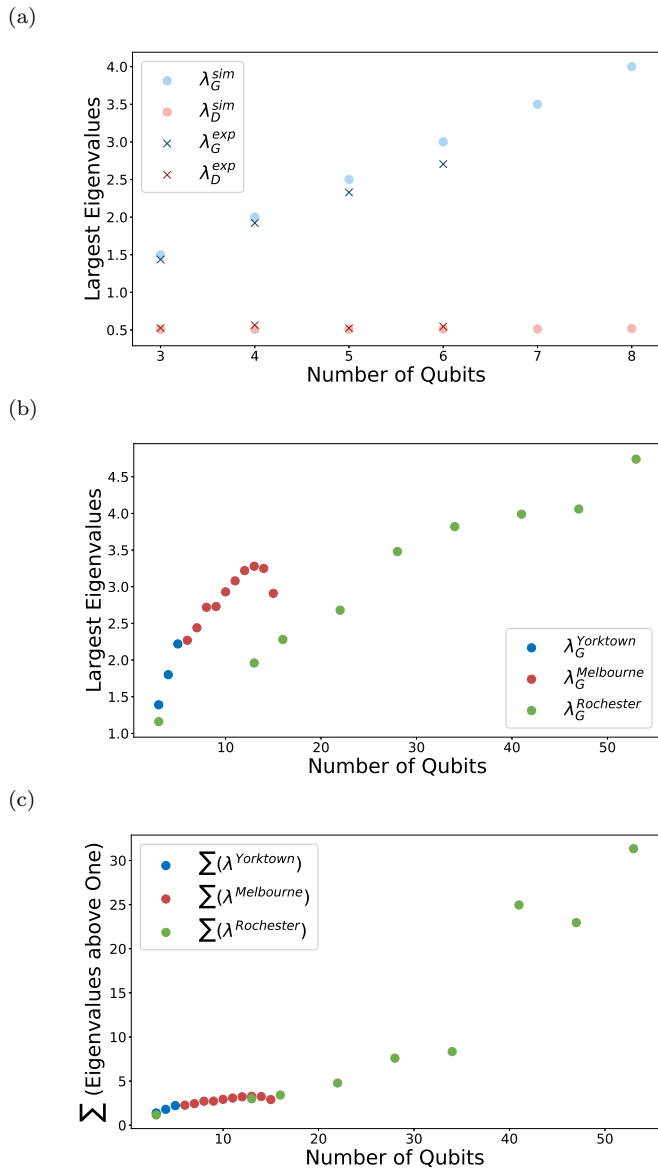


FIG. 3: **Exciton Condensation in the GHZ State.**

(a) The largest eigenvalue of the ${}^2\tilde{G}$ matrix (blue) and the 2D matrix (red) are shown for simulated (dots) and all mitigated, experimental (\times 's) calculations. (b) The largest eigenvalue of the unmitigated, experimental ${}^2\tilde{G}$ matrix and the (c) sum of all eigenvalues of the unmitigated, experimental ${}^2\tilde{G}$ matrix demonstrating exciton condensation ($\lambda > 1$) for experiments of N qubits on the Yorktown 5-qubits IBM Quantum Experience device (blue), the Melbourne 15-qubit IBM Quantum Experience device (red), and the Rochester 53-qubit IBM Quantum Experience device (green) are shown.

Discussion and Conclusions:

In this study, we have prepared molecular-scale exci-

ton condensates for three- to fifty-three-qubit systems on three quantum computers and verified the presence of the condensation through post-measurement computation of the exciton condensate's quantum signature [19]. The maximal condensate character is observed for the Greenberg-Horne-Zeilinger (GHZ) “maximally-entangled” state, indicating that a characteristic of this maximally-entanglement state is the entanglement of particle-hole pairs (excitons). Further, as the transmon qubit quantum states are occupied by microwave photons, the exciton condensate formed by preparation of the GHZ state corresponds to an exciton condensate of photons—the entanglement of photon-hole pairs. Whether photon-hole pair condensation would have similar properties to those of traditional fermion-hole exciton condensates is unknown, but it seems likely that, as the photons are directly analogous to fermions in a traditional exciton condensate, the superfluidity of photon-hole excitons should allow for the dissipationless flow of energy, which has possible applications in energy transport.

Additionally, the recognition of the GHZ state as an exciton condensate on a quantum computer establishes a new avenue for the creation and characterization of exciton condensates. As the GHZ state can be remotely and reliably constructed and probed through the use of cloud-accessible quantum devices, this preparation of exciton condensation may be more convenient than prior experimental methodologies. Moreover, depending on the type of qubit comprising the quantum device employed for a given experiment, various types of exciton condensates can be prepared. As quantum devices are created with a larger number of qubits, preparation of these higher-qubit GHZ states would create more macroscopically-scaled exciton condensates of these various compositions, although—as we have demonstrated—unless sufficient effort is done to prevent dispersion, this condensate character will be scattered throughout multiple eigenstates of the particle-hole RDM. Thus, future exploration of the properties of exciton condensates on quantum computers is anticipated, and the creation and characterization of exciton condensates is yet another motivation for the development of low-error quantum devices with macroscopic numbers of qubits.

Methods:

We include details on the quantum algorithms used to prepare the qubit states presented in the article; the quantum tomography of the modified particle-hole reduced density matrix; the methodology by which error is mitigated; and relevant details on the experimental quantum devices employed.

Quantum algorithms for state preparation. Two algorithms are utilized in this work to prepare the qubit states.

Minimalistic, Scanning Approach—The first algorithm takes a minimalistic approach to span all valid one-qubit occupation numbers for a three qubit system and is given

as follows:

$$|\Psi\rangle = C_3^2 R_{y,3}(\theta_3) C_1^2 R_{y,1}(\theta_2) C_1^3 R_{y,1}(\theta_1) |0\rangle^{\otimes 3}, \quad (10)$$

where $R_{y,i}$ refers to rotation of a qubit i about its Bloch sphere's y-axis—which is given by

$$R_{y,i} = \begin{pmatrix} \cos\left(\frac{\theta}{2}\right) & -\sin\left(\frac{\theta}{2}\right) \\ \sin\left(\frac{\theta}{2}\right) & \cos\left(\frac{\theta}{2}\right) \end{pmatrix} \quad (11)$$

—and C_i^j is a standard controlled-NOT (CNOT) gate with control and target qubits i and j respectively. Note that the control qubit is rotated prior to the application of the CNOT transformation. Overall, the sequence of transformations in Eq. (10) yields a wavefunction of the form

$$|\Psi\rangle = \alpha|000\rangle + \beta|011\rangle + \gamma|101\rangle + \delta|110\rangle, \quad (12)$$

such that α , β , γ , and δ are functions of the input angles $(\theta_1, \theta_2, \theta_3)$ and the 1-RDM contains solely diagonal elements.

The GHZ State—The GHZ State described in Eq. (9) is prepared according to

$$|\Psi\rangle = C_{N-1}^N \cdots C_2^3 C_1^2 H_1 |0\rangle^{\otimes N} \quad (13)$$

for an N -qubit state where H_i represents the Hadamard gate—which maps $|0\rangle$ to $\frac{|0\rangle+|1\rangle}{\sqrt{2}}$ and $|1\rangle$ to $\frac{|0\rangle-|1\rangle}{\sqrt{2}}$ —acting on qubit i . There has been much study on the optimal preparation of the GHZ state for various numbers of qubits [36]; in this study, however, the simple algorithm from Ref. 37 for GHZ state preparation is utilized as it is easily implemented and generalizable to any arbitrary number of qubits.

Quantum tomography for the modified particle-hole RDM. The modified particle-hole RDM—with elements given by Eq. (3)—is obtained through the translation of all of its elements into the bases of Pauli matrices, which are directly probed on the quantum computer.

First, let us focus on the ${}^1D_i^j$ terms of the ${}^2\tilde{G}$ matrix elements. As 1-RDMs simplify to block-diagonal forms with respect to single qubits, there are no non-zero two-qubit 1-RDM terms. In order for a 1-RDM to be non-zero, then, it must be a one-qubit 1-RDM of the form

$$\begin{array}{c|cc} & \hat{a}_{p,0} & \hat{a}_{p,1} \\ \hline \hat{a}_{p,0}^\dagger & \hat{a}_{p,0}^\dagger \hat{a}_{p,0} & \hat{a}_{p,0}^\dagger \hat{a}_{p,1} \\ \hat{a}_{p,1}^\dagger & \hat{a}_{p,1}^\dagger \hat{a}_{p,0} & \hat{a}_{p,1}^\dagger \hat{a}_{p,1} \end{array} \quad (14)$$

for qubit p where \hat{a}_p^\dagger and \hat{a}_p are creation and annihilation operators for qubit p , respectively. Each term of these non-zero, one-qubit 1-RDMs can be written as a linear combination of Pauli matrices. For example, $\hat{a}_{p,0}^\dagger \hat{a}_{p,1}$ —which represents the qubit going from state $|1\rangle = \begin{pmatrix} 0 \\ 1 \end{pmatrix}$ to state $|0\rangle = \begin{pmatrix} 1 \\ 0 \end{pmatrix}$ —can be written as follows:

$$\hat{a}_{p,0}^\dagger \hat{a}_{p,1} = \begin{pmatrix} 0 & 1 \\ 0 & 0 \end{pmatrix} = \frac{1}{2} (X_p + iY_p). \quad (15)$$

Similarly, the other elements can be represented as shown:

$$\hat{a}_{p,1}^\dagger \hat{a}_{p,0} = \begin{pmatrix} 0 & 0 \\ 1 & 0 \end{pmatrix} = \frac{1}{2} (X_p - iY_p), \quad (16)$$

$$\hat{a}_{p,0}^\dagger \hat{a}_{p,0} = \begin{pmatrix} 1 & 0 \\ 0 & 0 \end{pmatrix} = \frac{1}{2} (\hat{I} + Z_p), \quad (17)$$

$$\hat{a}_{p,1}^\dagger \hat{a}_{p,1} = \begin{pmatrix} 0 & 0 \\ 0 & 1 \end{pmatrix} = \frac{1}{2} (\hat{I} - Z_p). \quad (18)$$

The expectation value of each matrix element for a given qubit (p) can then be obtained by directly probing the expectation values of X_p , Y_p , and Z_p for a given state preparation.

The overall particle-hole RDM (2G matrix) can be represented as a $4N \times 4N$ matrix composed of N^2 4×4 sub-matrices of the form

$$\begin{array}{c|cccc} & \hat{a}_{q,0}^\dagger \hat{a}_{q,0} & \hat{a}_{q,1}^\dagger \hat{a}_{q,0} & \hat{a}_{q,0}^\dagger \hat{a}_{q,1} & \hat{a}_{q,1}^\dagger \hat{a}_{q,1} \\ \hline \hat{a}_{p,0}^\dagger \hat{a}_{p,0} & \hat{a}_{p,0}^\dagger \hat{a}_{p,0} \hat{a}_{q,0}^\dagger \hat{a}_{q,0} & \hat{a}_{p,0}^\dagger \hat{a}_{p,0} \hat{a}_{q,1}^\dagger \hat{a}_{q,0} & \hat{a}_{p,0}^\dagger \hat{a}_{p,0} \hat{a}_{q,0}^\dagger \hat{a}_{q,1} & \hat{a}_{p,0}^\dagger \hat{a}_{p,0} \hat{a}_{q,1}^\dagger \hat{a}_{q,1} \\ \hat{a}_{p,0}^\dagger \hat{a}_{p,1} & \hat{a}_{p,0}^\dagger \hat{a}_{p,1} \hat{a}_{q,0}^\dagger \hat{a}_{q,0} & \hat{a}_{p,0}^\dagger \hat{a}_{p,1} \hat{a}_{q,1}^\dagger \hat{a}_{q,0} & \hat{a}_{p,0}^\dagger \hat{a}_{p,1} \hat{a}_{q,0}^\dagger \hat{a}_{q,1} & \hat{a}_{p,0}^\dagger \hat{a}_{p,1} \hat{a}_{q,1}^\dagger \hat{a}_{q,1} \\ \hat{a}_{p,1}^\dagger \hat{a}_{p,0} & \hat{a}_{p,1}^\dagger \hat{a}_{p,0} \hat{a}_{q,0}^\dagger \hat{a}_{q,0} & \hat{a}_{p,1}^\dagger \hat{a}_{p,0} \hat{a}_{q,1}^\dagger \hat{a}_{q,0} & \hat{a}_{p,1}^\dagger \hat{a}_{p,0} \hat{a}_{q,0}^\dagger \hat{a}_{q,1} & \hat{a}_{p,1}^\dagger \hat{a}_{p,0} \hat{a}_{q,1}^\dagger \hat{a}_{q,1} \\ \hat{a}_{p,1}^\dagger \hat{a}_{p,1} & \hat{a}_{p,1}^\dagger \hat{a}_{p,1} \hat{a}_{q,0}^\dagger \hat{a}_{q,0} & \hat{a}_{p,1}^\dagger \hat{a}_{p,1} \hat{a}_{q,1}^\dagger \hat{a}_{q,0} & \hat{a}_{p,1}^\dagger \hat{a}_{p,1} \hat{a}_{q,0}^\dagger \hat{a}_{q,1} & \hat{a}_{p,1}^\dagger \hat{a}_{p,1} \hat{a}_{q,1}^\dagger \hat{a}_{q,1} \end{array} \quad (19)$$

where each element of the matrix is the expectation value of the creation and annihilation operator terms shown. As multi-qubit wavefunctions are the tensor products of individual qubit wavefunctions, these four-body terms can be represented as the tensor products of the two-body terms composing them. For example, the expectation value of the term $\hat{a}_{p,0}^\dagger \hat{a}_{p,1} \hat{a}_{q,1}^\dagger \hat{a}_{q,1}$ can be written as

$$\frac{1}{4} \left[\langle X_p \otimes \hat{I}_q \rangle - \langle X_p \otimes Z_q \rangle + i \langle Y_p \otimes \hat{I}_q \rangle - i \langle Y_p \otimes Z_q \rangle \right], \quad (20)$$

where $\langle Y_p \otimes Z_q \rangle$ is one of nine two-qubit expectation values that can be obtained from quantum computation. All other terms can be determined using analogous, straightforward methodologies.

Similarly, the overall modified particle-hole RDM (${}^2\tilde{G}$ matrix) can be represented as a $4N \times 4N$ matrix composed of N^2 4×4 sub-matrices. These sub-matrices are identical to the sub-matrices of the 2G matrix with the block modification shown below subtracted off to eliminate the extraneous ground-state-to-ground-state transition:

$$\begin{array}{c|cccc} & \hat{a}_{q,0}^\dagger \hat{a}_{q,0} & \hat{a}_{q,1}^\dagger \hat{a}_{q,0} & \hat{a}_{q,0}^\dagger \hat{a}_{q,1} & \hat{a}_{q,1}^\dagger \hat{a}_{q,1} \\ \hline \hat{a}_{p,0}^\dagger \hat{a}_{p,0} & {}^1D_i[0,0] {}^1D_j[0,0] & {}^1D_i[0,0] {}^1D_j[0,1] & {}^1D_i[0,0] {}^1D_j[1,0] & {}^1D_i[0,0] {}^1D_j[1,1] \\ \hat{a}_{p,0}^\dagger \hat{a}_{p,1} & {}^1D_i[0,1] {}^1D_j[0,0] & {}^1D_i[0,1] {}^1D_j[0,1] & {}^1D_i[0,1] {}^1D_j[1,0] & {}^1D_i[0,1] {}^1D_j[1,1] \\ \hat{a}_{p,1}^\dagger \hat{a}_{p,0} & {}^1D_i[1,0] {}^1D_j[0,0] & {}^1D_i[1,0] {}^1D_j[0,1] & {}^1D_i[1,0] {}^1D_j[1,0] & {}^1D_i[1,0] {}^1D_j[1,1] \\ \hat{a}_{p,1}^\dagger \hat{a}_{p,1} & {}^1D_i[1,1] {}^1D_j[0,0] & {}^1D_i[1,1] {}^1D_j[0,1] & {}^1D_i[1,1] {}^1D_j[1,0] & {}^1D_i[1,1] {}^1D_j[1,1] \end{array} \quad (21)$$

Note that 1D_i is the RDM for qubit i described in Eq. (14) and that ${}^1D_i[a, b]$ is the element of that matrix with matrix coordinates $[a, b]$.

The overall form of the ${}^2\tilde{G}$ matrix is hence

$$(22) \quad \begin{array}{|c|c|c|c|} \hline p=0, q=0 & p=0, q=1 & \cdots & p=0, q=N-1 \\ \hline p=1, q=0 & p=1, q=1 & \cdots & p=1, q=N-1 \\ \hline \vdots & \vdots & \ddots & \vdots \\ \hline p=N-1, q=0 & p=N-1, q=1 & \cdots & p=N-1, q=N-1 \\ \hline \end{array}$$

where each p/q combination represents one of the previously-specified blocks, i.e., the difference of the matrices given in Eqs. (19) and (21). The largest eigenvalue of this overall matrix is the λ_G value employed throughout this article.

As the states prepared in this study are real wavefunctions, the imaginary components of the RDMs should be approximately zero within a small range dictated by inherent randomness and by the error of the devices. Therefore, only the five of the possible nine two-qubit expectation values that correspond to real contributions to the RDMs [$\langle X_p \otimes X_q \rangle$, $\langle Y_p \otimes Y_q \rangle$, $\langle Z_p \otimes Z_q \rangle$, $\langle X_p \otimes Z_q \rangle$, and $\langle Z_p \otimes X_q \rangle$] are non-zero and hence essential for construction of the ${}^2\tilde{G}$ matrix. While, for the sake of completeness, the negligibly-small imaginary components are included in the construction of the ${}^2\tilde{G}$ matrix for the low-qubit ($N = 3 - 5$) computations, only real components are included in the ${}^2\tilde{G}$ matrix for higher-qubit ($N = 6 - 15$) computations to lower computational expense.

Error mitigation. A measurement correction fitter for a tensored calibration is employed to mitigate measurement error through use of the “least squares” method—that constrains the resultant mitigated counts to having physical probabilities—to construct a mitigation filter that can be applied to experimental data.

Experimental quantum device specifications.

Throughout this work, we employ the `ibmqx2` (`ibmq_5_yorktown`) [38], the `ibmq_16_melbourne` [39], and the `ibmq_rochester` [40] IBM Quantum Experience devices, which are available online. Unless explicitly stated otherwise, all low-qubit ($N \leq 5$) experiments are conducted using the five-qubit `ibmqx2` (`ibmq_5_yorktown`) device, all midrange-qubit ($5 < N \leq 15$) experiments are conducted using the fifteen-qubit `ibmq_16_melbourne` device, and all high-qubit ($N > 15$) experiments are conducted using the fifty-three-qubit `ibmq_rochester` device. These quantum devices are composed of fixed-frequency transmon qubits with co-planer waveguide resonators [41, 42]. Experimental calibration data and connectivity for these devices are included in the Supporting Information.

ACKNOWLEDGMENTS

Acknowledgments: The authors acknowledge use of the IBM Q for this work. D.A.M. gratefully acknowledges the Department of Energy, Office of Basic Energy Sciences, Grant [de-sc0019215](#), the U.S. National Science Foundation Grant No. CHE-1565638 and the U.S. Army Research Office (ARO) Grant No. W911NF-16-1-0152. The views expressed are of the authors and do not reflect the official policy or position of IBM or the IBM Q team.

Author contributions. D. A. M. conceived of the project. L.M.S. performed the computations on the quantum computers. L.M.S., S.E.S., and D.A.M. analyzed the data and wrote the manuscript.

Competing interests. The authors do not have competing interests.

Materials & Correspondence. D. A. M. is the corresponding author at damaz@uchicago.edu.

-
- [1] D. V. Fil and S. I. Shevchenko, “Electron-hole superconductivity (review),” *Low Temp. Phys.* **44**, 867–909 (2018).
- [2] L. V. Keldysh, “Coherent states of excitons,” *Physics-Uspekhi* **60**, 11801186 (2017).
- [3] M. Kellogg, J. P. Eisenstein, L. N. Pfeiffer, and K. W. West, “Vanishing Hall resistance at high magnetic field in a double-layer two-dimensional electron system,” *Phys. Rev. Lett.* **93**, 036801 (2004).
- [4] E. Tutuc, M. Shayegan, and D. A. Huse, “Counterflow measurements in strongly correlated GaAs hole bilayers: evidence for electron-hole pairing,” *Phys. Rev. Lett.* **93**, 36802 (2004).
- [5] S. Safaei and D. A. Mazziotti, “Quantum signature of exciton condensation,” *Phys. Rev. B* **98**, 045122 (2018).
- [6] A. Kogar, M. S. Rak, S. Vig, A. A. Husain, F. Flicker, Y. I. Joe, L. Venema, G. J. MacDougall, T. C. Chiang, E. Fradkin, J. van Wezel, and P. Abbamonte, “Signatures of exciton condensation in a transition metal dichalcogenide,” *Science* **358**, 1314–1317 (2017).
- [7] X. Liu, K. Watanabe, T. Taniguchi, B. I. Halperin, and P. Kim, “Quantum Hall drag of exciton condensate in graphene,” *Nat. Phys.* **13**, 746–750 (2017).
- [8] D. Varsano, S. Sorella, D. Sangalli, M. Barborini, S. Corni, E. Molinari, and M. Rontani, “Carbon nanotubes as excitonic insulators,” *Nature Communications* **8** (2017).
- [9] J. Kasprzak, M. Richard, S. Kundermann, A. Baas, P. Jembrun, J. M. J. Keeling, F. M. Marchetti, M. H. Szymanska, R. André, J. L. Staehli, V. Savona, P. B. Littlewood, B. Deveaud, and Le Si Dang, “Bose-Einstein condensation of exciton polaritons,” *Nature* **443**, 409 (2006).
- [10] M. S. Fuhrer and A. R. Hamilton, “Chasing the exciton condensate,” *Physics* **9** (2016).
- [11] I. B. Spielman, J. P. Eisenstein, L. N. Pfeiffer, and K. W. West, “Resonantly enhanced tunneling in a double layer quantum Hall ferromagnet,” *Phys. Rev. Lett.* **84**, 5808–5811 (2000).
- [12] D. Nandi, A. D. K. Finck, J. P. Eisenstein, L. N. Pfeiffer, and K. W. West, “Exciton condensation and perfect Coulomb drag,” *Nature* **488**, 481–484 (2012).

- [13] R. Ma, B. Saxberg, C. Owens, N. Leung, Y. Lu, J. Simon, and D. I. Schuster, “A dissipatively stabilized Mott insulator of photons,” *Nature* **566**, 5157 (2019).
- [14] H. J. Lipkin, N. Meshkov, and A. J. Glick, “Validity of many-body approximation methods for a solvable model: (i.) exact solutions and perturbation theory,” *Nucl. Phys. A* **62**, 188–198 (1965).
- [15] R. Pérez, M. C. Cambiaggio, and J. P. Vary, “t expansion and the Lipkin model,” *Phys. Rev. C* **37**, 2194–2198 (1988).
- [16] D. A. Mazziotti, “Contracted Schrödinger equation: determining quantum energies and two-particle density matrices without wave functions,” *Phys. Rev. A* **57**, 4219–4234 (1998).
- [17] J. Stein, “Unitary flow of the bosonized large-N Lipkin model,” *J. Phys. G Nucl. Part. Phys.* **26**, 377–385 (2000).
- [18] D. A. Mazziotti, “Exactness of wave functions from two-body exponential transformations in many-body quantum theory,” *Phys. Rev. A* **69**, 012507 (2004).
- [19] C. Garrod and M. Rosina, “Particlehole matrix: its connection with the symmetries and collective features of the ground state,” *J. Math. Phys.* **10**, 1855–1861 (1969).
- [20] S. N. Bose and A. Einstein, “Planck’s law and light quantum hypothesis,” *Zeitschrift für Physik* **26**, 178 (1924).
- [21] A. Einstein, “Quantentheorie des einatomigen idealen gases,” *K.P.A.W.*, 261267 (1924).
- [22] F. London, “On Bose-Einstein condensation,” *Phys. Rev.* **54**, 947–954 (1938).
- [23] L. Tisza, “The theory of liquid helium,” *Phys. Rev.* **72**, 838–854 (1947).
- [24] W. Pauli, “The connection between spin and statistics,” *Physical Review* **58**, 716722 (1940).
- [25] P. W. Anderson, “Twenty-five years of high-temperature superconductivity – a personal review,” *J. Phys.: Conf. Ser.* **449**, 012001 (2013).
- [26] C. N. Yang, “Concept of off-diagonal long-range order and the quantum phases of liquid He and of superconductors,” *Rev. Mod. Phys.* **34**, 694–704 (1962).
- [27] F. Sasaki, “Eigenvalues of fermion density matrices,” *Phys. Rev.* **138**, B1338–B1342 (1965).
- [28] W. Kohn and D. Sherrington, “Two kinds of bosons and bose condensates,” *Rev. Mod. Phys.* **42**, 1–11 (1970).
- [29] S. E. Smart, D. I. Schuster, and D. A. Mazziotti, “Experimental data from a quantum computer verifies the generalized Pauli exclusion principle,” *Communications Physics* **2** (2019).
- [30] R. E. Borland and K. Dennis, “The conditions on the one-matrix for three-body fermion wavefunctions with one-rank equal to six,” *J. Phys. B: At. Mol. Opt. Phys.* **5**, 715 (1972).
- [31] C. Schilling, D. Gross, and M. Christandl, “Pinning of fermionic occupation numbers,” *Physical Review Letters* **110** (2013).
- [32] C. L. Benavides-Riveros, J. M. Gracia-Bonda, and M. Springborg, “Quasipinning and entanglement in the lithium isoelectronic series,” *Physical Review A* **88** (2013).
- [33] R. Chakraborty and D. A. Mazziotti, “Generalized pauli conditions on the spectra of one-electron reduced density matrices of atoms and molecules,” *Physical Review A* **89** (2014).
- [34] D. A. Mazziotti, “Pure-N-representability conditions of two-fermion reduced density matrices,” *Physical Review A* **94** (2016).
- [35] M. Walter, D. Gross, and J. Eisert, “Multipartite entanglement,” *Quantum Information*, 293330 (2016).
- [36] D. Cruz, R. Fournier, F. Gremion, A. Jeannerot, K. Komagata, T. Tosić, J. Thiesbrummel, C. L. Chan, N. Macris, M.-A. Dupertuis, and C. Javerzac-Galy, “Efficient quantum algorithms for ghz and w states, and implementation on the ibm quantum computer,” *Advanced Quantum Technologies* **2**, 1900015 (2019).
- [37] M. Treinish and D. M. Rodriguez, “GHZ state example,” [GitHub](#).
- [38] IBM-Q-Team, “IBM-Q-5 Yorktown backend specification v2.0.0,” (2019).
- [39] IBM-Q-Team, “IBM-Q-15 Melbourne backend specification v2.0.0,” (2019).
- [40] IBM-Q-Team, “IBM-Q-53 Rochester backend specification v1.2.0,” (2020).
- [41] J. Koch, T. M. Yu, J. Gambetta, A. A. Houck, D. I. Schuster, J. Majer, A. Blais, M. H. Devoret, S. M. Girvin, R. J. Schoelkopf, and et. al., “Charge-insensitive qubit design derived from the cooper pair box,” *Physical Review A* **76** (2007).
- [42] J. M. Chow, A. D. Crocoles, J. M. Gambetta, C. Rigetti, B. R. Johnson, J. A. Smolin, J. R. Rozen, G. A. Keefe, M. B. Rothwell, M. B. Ketchen, and et al., “Simple all-microwave entangling gate for fixed-frequency superconducting qubits,” *Physical Review Letters* **107** (2011).